TEMPERATURE MEASUREMENTS IN FLOWING WATER: VISCOUS HEATING OF SENSOR TIPS

1st IGHEM Meeting, Montreal, Canada
June 1996

Nordeen Larson and Arthur M. Pederson
Sea-Bird Electronics, Inc, 1808 136th Place NE
Bellevue, WA 98005-2389 USA

internet: seabird@seabird.com

Introduction

Sea-Bird Electronics manufactures instruments for oceanographic research, specializing in temperature, pressure and salinity measurement. We have a keen interest in measurement. As such, we not only work to improve instrument design but to understand the limitations of field measurement and to refine the use of instruments and methods of measurement.

The magnitude of temperature errors in the presence of flow became evident in measurements of ocean salinity. Salinity is computed from temperature, conductivity, and pressure measurements that must be coordinated on the same parcel of water. To accomplish this the water is drawn past temperature and conductivity sensors in a duct where the flow is carefully controlled by a pump. In Figure 1 the temperature difference between two independently pumped temperature sensors changes when the flow is slowed past the first sensor (A), then restored (B), then flow is slowed past the second sensor (C), and then restored (D).

The temperature measurements in this flow stream register too warm due to viscous heating of the probe tip. The error is of order 0.001 °C at 1 m/s and increases as the square root of Prandtl number and velocity squared. It varies mildly with the angle of attack (< 15%) and probe shape (< 5%). Based on Prandtl number scaling, the error should be greatest in laminar flows and decrease with embedded turbulence by up to a factor of 3 in 0°C water.

In turbine efficiency measurements as well as oceanography where mK precision is required, measurement methods must be developed to allow the flow-induced viscous heating errors to be characterized and removed from data. Toward this goal, Sea-Bird has been investigating viscous heating effects with computational fluid dynamics (CFD) models and direct laboratory measurements.

three notable features; no heating at the stagnation point, a peak in heating under the region of accelerated flow, and a near constant skin temperature under the down-stream boundary layer. The skin temperature of water along the probe surface rises through a peak and settles to a constant value (Figure 7).

The 'over'-temperature experienced by the thermistor bead inside the metal probe sheath is an average of the skin temperature from the probe tip back perhaps 1 to 3 bead diameters (sheath diameters). This area-weighted average temperature is the second curve (Figure 7). At two diameters back from the probe tip the average temperature is within 0.1 mK (5%) of the temperature averaged for 10 diameters back (dashed asymptote).

Using the average probe tip temperature from computational runs at several velocities, temperatures, and pressure (Figure 8), the over-temperature is found to vary exactly as (Figure 9)

CFD over-temperature = 1.263e-4 * (Pr)^0.5 * (U)^2 $\approx$ 0.339 * (ν)^0.5 * (U)^2

U = free stream velocity

Pr = Prandtl number = ($\nu \rho$ Cp / κ)

ν = kinematic viscosity

ρ = density

Cp = heat capacity

κ = thermal conductivity

It is apparent that the downstream boundary layer keeps the probe surface temperature remarkably constant. The assumption of small stem-conduction losses of heat down the probe metal sheath would seem to be reasonable. There is very little surface temperature forcing to drive heat down the sheath and local viscous heating at distances down the probe length balance any stem losses.

Sensor tip geometry

The over-temperature of the probe tip is not very sensitive to tip geometry. Two alternate tip shapes were modeled (Figure 10); a blunted nose (A), and a more stream-lined elliptical tip geometry (B). While the specific temperature distribution at the probe tip is different within the first diameter, the area-weighted average temperatures from all probe shapes agree to better than 5% when averaged 1 or more diameters back from the tip (Figure 11).

Isothermal wall approximation

To investigate the effect of heat redistribution by the sensor metal sheath, the next computational approximation was to consider heat flux through the sheath wall. We assume that the net flux of heat through the probe surface is zero, and that the metal sheath reaches a constant temperature. This is likely satisfied by the higher thermal conductivity of metal (ν=14.6) than water (ν=0.59) and low stem-conduction losses due to the probe length (50 diameters length and small metal crossectional area). Computational runs, at constant flow conditions, are iterated until a probe surface temperature is found which results in a zero net heat flux through the probe surface (forward 11 diameters of the model).

The 'over'-temperature experienced by a thermistor bead inside the metal probe sheath is an average of the surface temperature around the cylinder. The area-weighted average temperature is the second curve and yields about 1.2 mK above ambient at 2 m/s in contrast to 1.9 mK in the axisymmetric case. The adiabatic wall may not be a good approximation for this flow orientation because heat is likely to redistribute quickly and efficiently along the short circumferential path in the probe metal sheath.

The over-temperature has the same functional dependence on flow speed and viscosity as in the axisymmetric geometry but with a smaller scaling coefficient for the adiabatic wall case.

$$\text{CFD over-temperature} = 0.797e\text{-}4 * (Pr)^{0.5} * (U)^2 \approx 0.214 * (\nu)^{0.5} * (U)^2$$

Isothermal wall approximation

In the perpendicular flow case the isothermal wall approximation is more applicable because of the short circumferential distances that heat can be easily transferred in the metal sheath wall. The same approach is taken where computational runs, at constant flow conditions, are iterated until a probe surface temperature is found which results in a zero net heat flux through the circumferential probe surface.

As in the axisymmetric case the heat flux distribution for three probe temperatures shows the anticipated form (Figure 19); a large heat flux into the probe surface under the region of accelerated flow at the upstream edge of the cylinder tip and out of the probe at the stagnation point and in the downstream wake. However, the average wall temperatures increase 30% above the adiabatic wall approximation because the wall in the wake region of the flow can be heated fairly effectively by spot heating at the upstream cylinder rim (Figure 20).

Extension of the Results to Turbulent flows

To date the CFD models have not been extended to full 3-dimensional flow, a requirement for meaningful computations of turbulent flows. However, the scaling of the viscous heating results with Prandtl number do predict a decrease in the wall temperature as turbulence develops within a constant mean flow and the Prandtl number decreases toward 1. The scaling for laminar flow on a flat plate goes as $(Pr)^{1/2}$, whereas for high speed turbulent air flows it goes as $(Pr)^{1/3}$ (Schlichting, 1979).

The Prandtl number of ocean water at 2°C is 12.4. The available scaling suggests a decrease in the wall temperature of a factor of 3.5 to 2.3 if turbulence embedded within a flow of this water drove the Prandtl number to 1.

Further investigation of the viscous heating effect in turbulent flows is probably necessary for a full understanding of the turbine efficiency monitoring application.

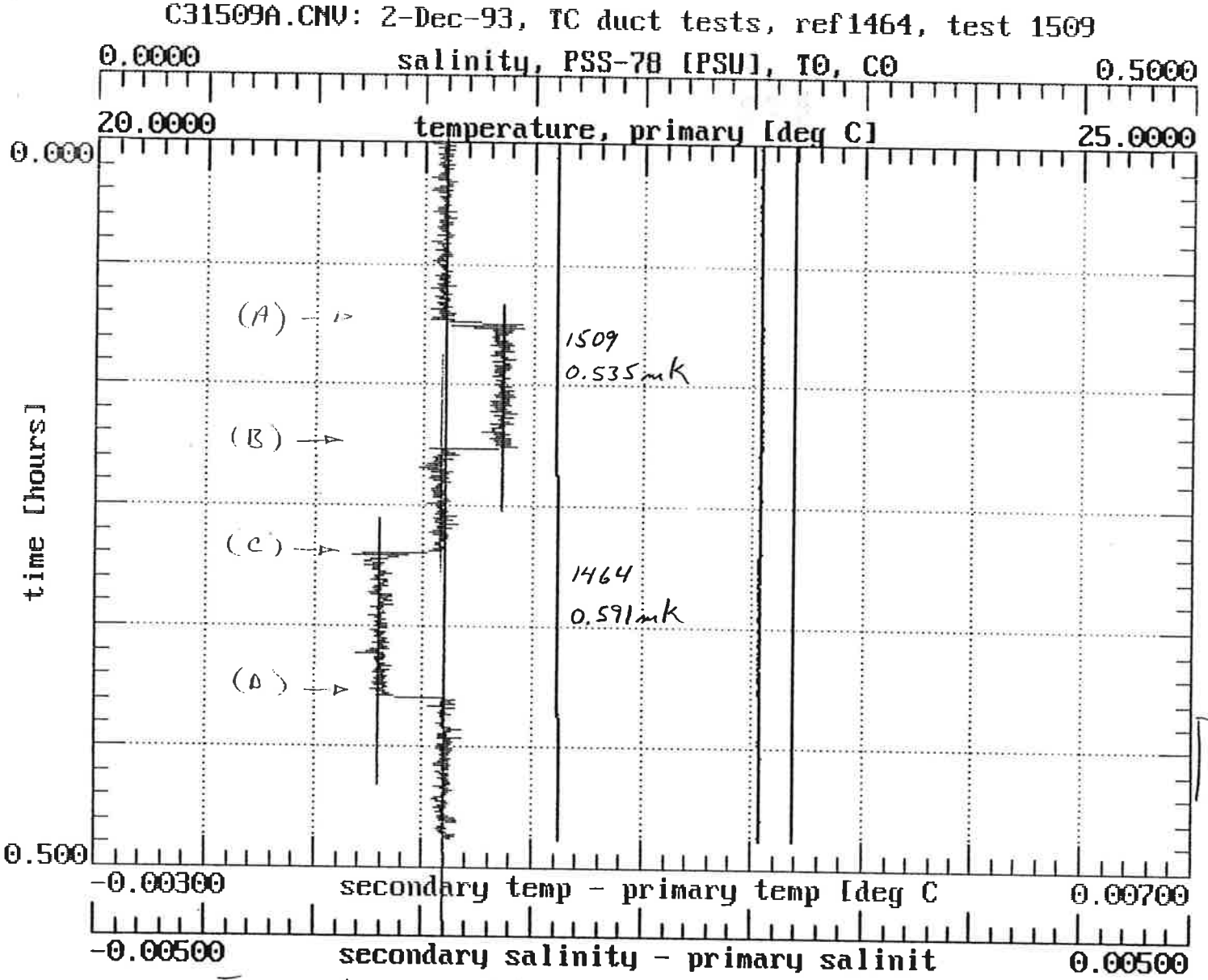

clean TC
run 3

$\bar{T}$ = 27.1°C

ν = 0.9569

$\bar{u}$ = 1.02 m/s

$\Delta\bar{T}$ = 0.563 mK

$\bar{T}$	ν	$\Delta\bar{T}$
27.1°C	.9569	0.563 mK
ϕ	1.7792	1.05 mK
+2,34.6	1.7172	1.01 mK
ϕ 74Lm	1.8230	1.08 mK

Figure 1

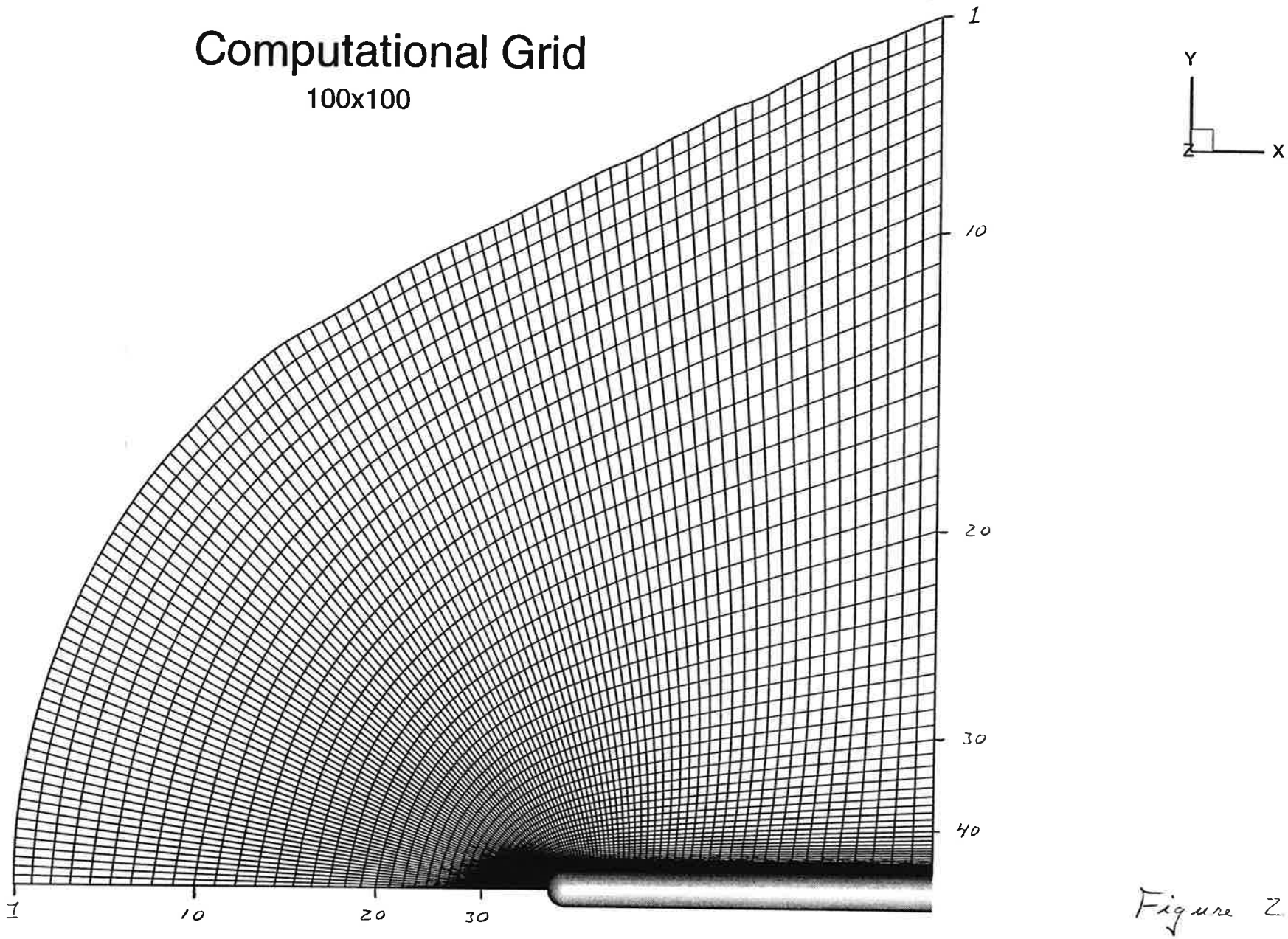

Figure 2

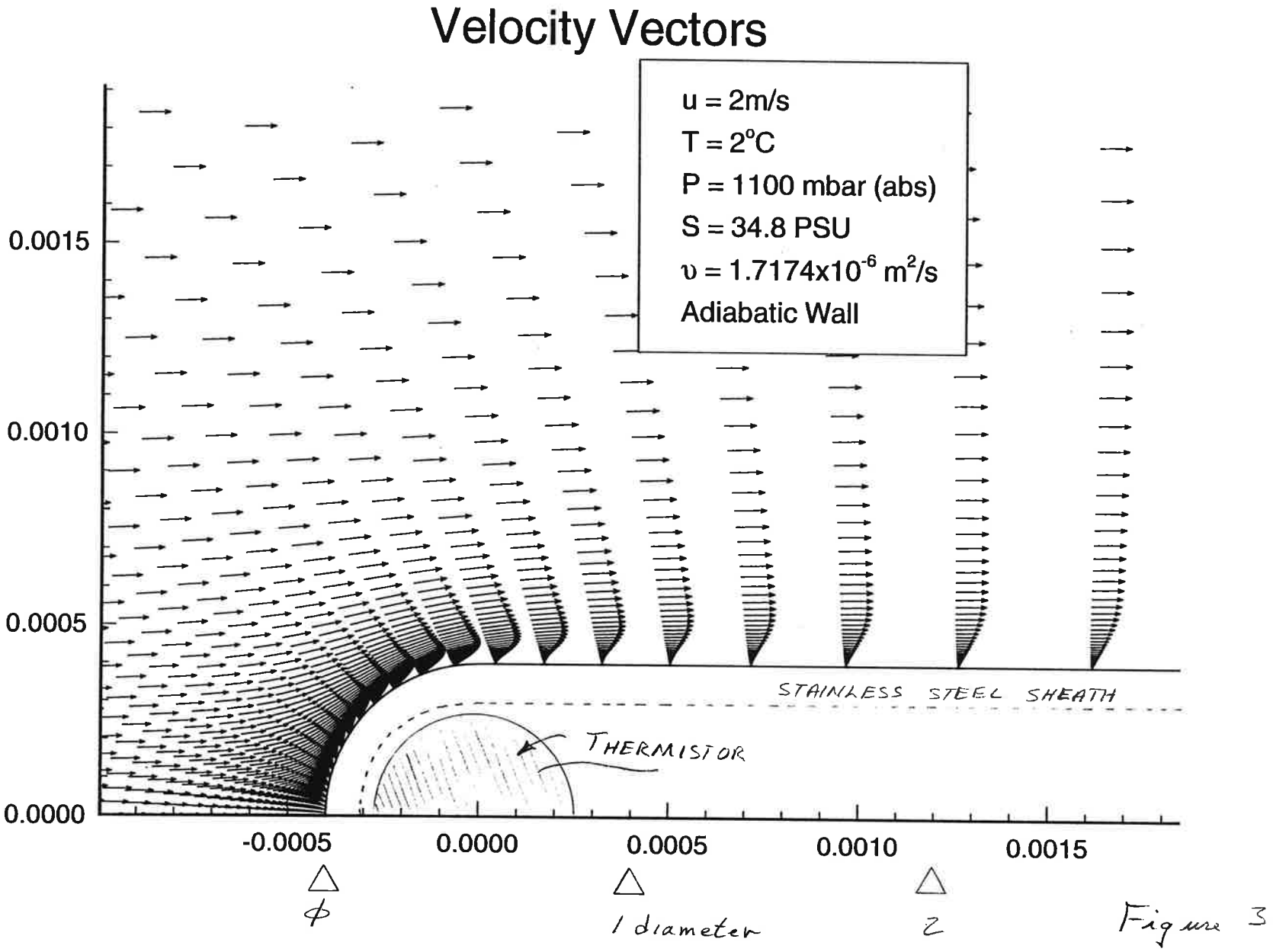
Velocity Vectors
u = 2m/s
T = 2°C
P = 1100 mbar (abs)
S = 34.8 PSU
υ = 1.7174x10-6 m2/s
Adiabatic Wall
0.0015
0.0010
0.0005
0.0000
STAINLESS STEEL SHEATH
THERMISTOR
-0.0005
0.0000
0.0005
0.0010
0.0015
φ
1 diameter
z

Figure 3

Velocity Magnitude Contours

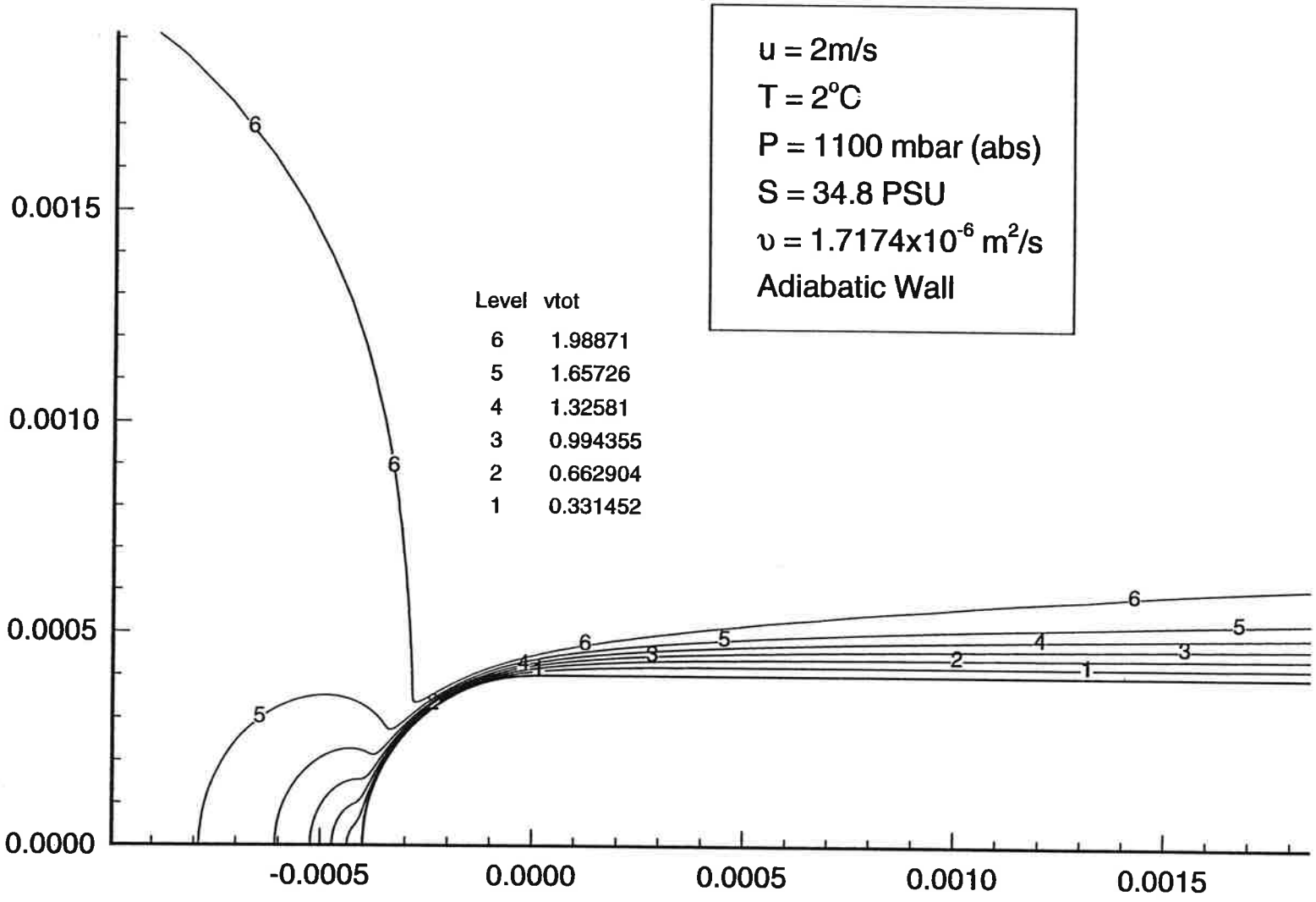

Figure 4

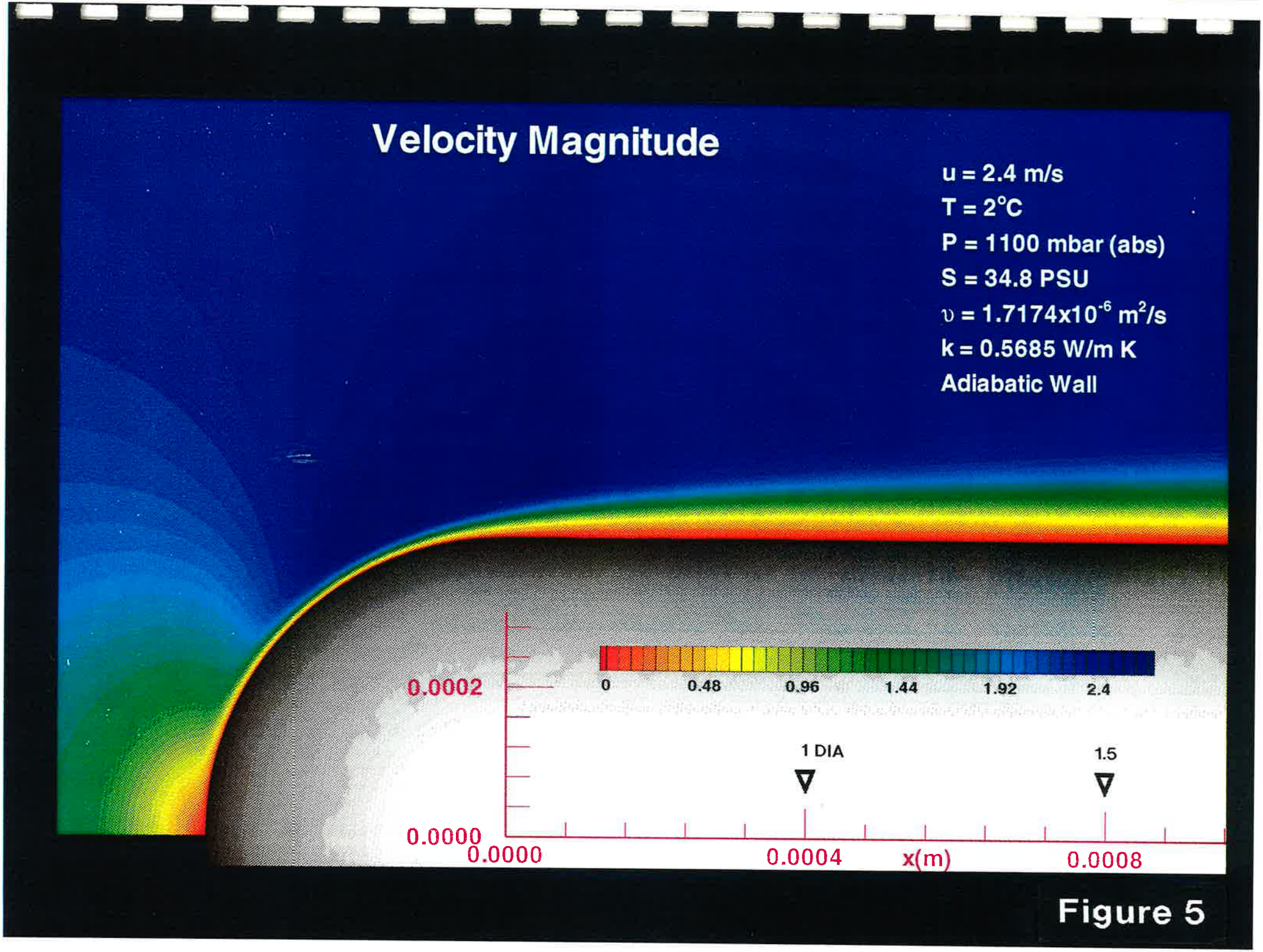
Velocity Magnitude
u = 2.4 m/s
T = 2°C
P = 1100 mbar (abs)
S = 34.8 PSU
υ = 1.7174x10^-6 m^2/s
k = 0.5685 W/m K
Adiabatic Wall
0
0.48
0.96
1.44
1.92
2.4
1 DIA
1.5
0.0002
0.0000
0.0000
0.0004
x(m)
0.0008

Figure 5

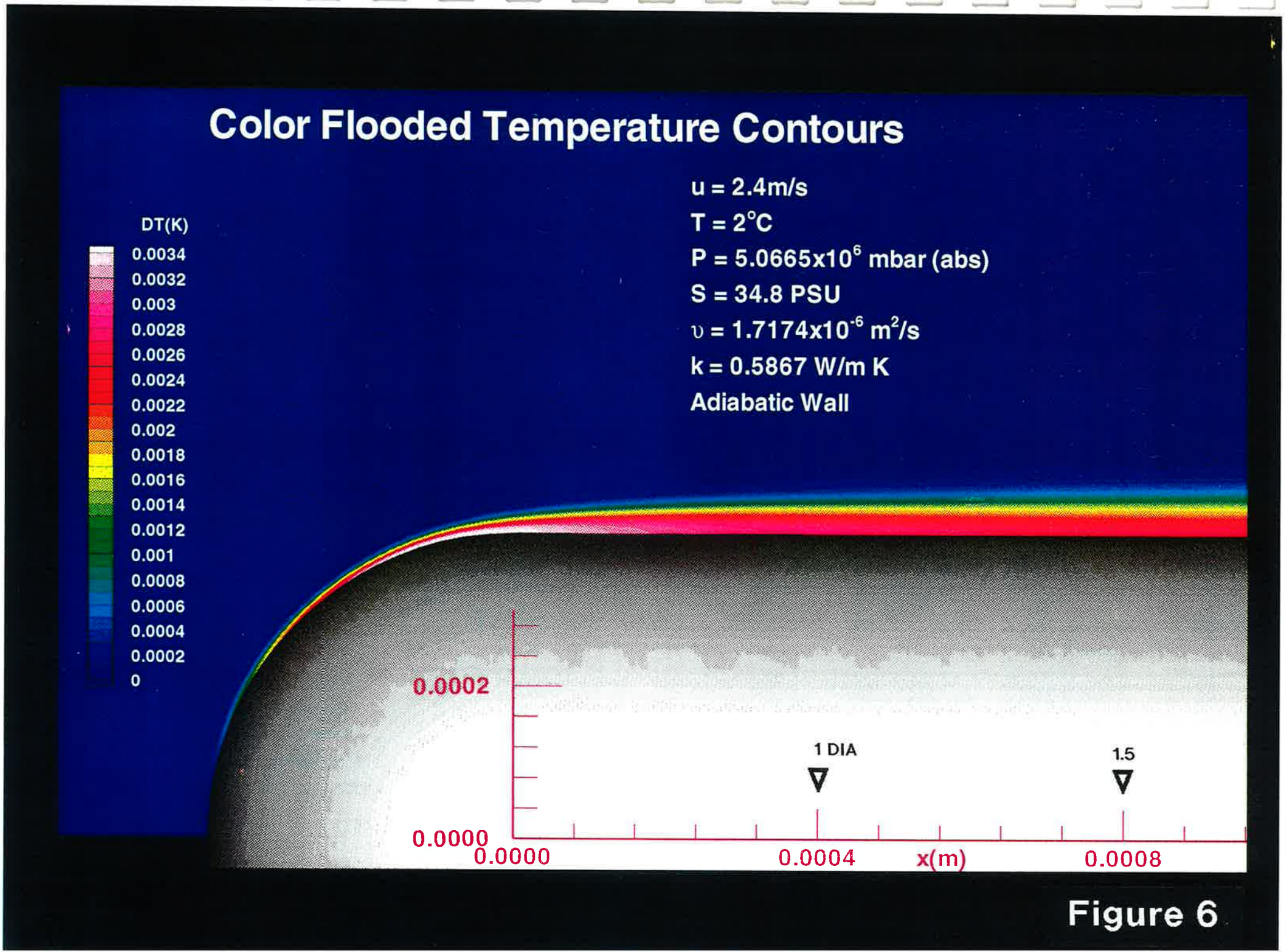
Color Flooded Temperature Contours
u = 2.4m/s
T = 2°C
P = 5.0665x10^6 mbar (abs)
S = 34.8 PSU
υ = 1.7174x10^-6 m^2/s
k = 0.5867 W/m K
Adiabatic Wall
DT(K)
0.0034
0.0032
0.003
0.0028
0.0026
0.0024
0.0022
0.002
0.0018
0.0016
0.0014
0.0012
0.001
0.0008
0.0006
0.0004
0.0002
0
0.0002
0.0000
0.0000
1 DIA
0.0004
x(m)
1.5
0.0008

Figure 6

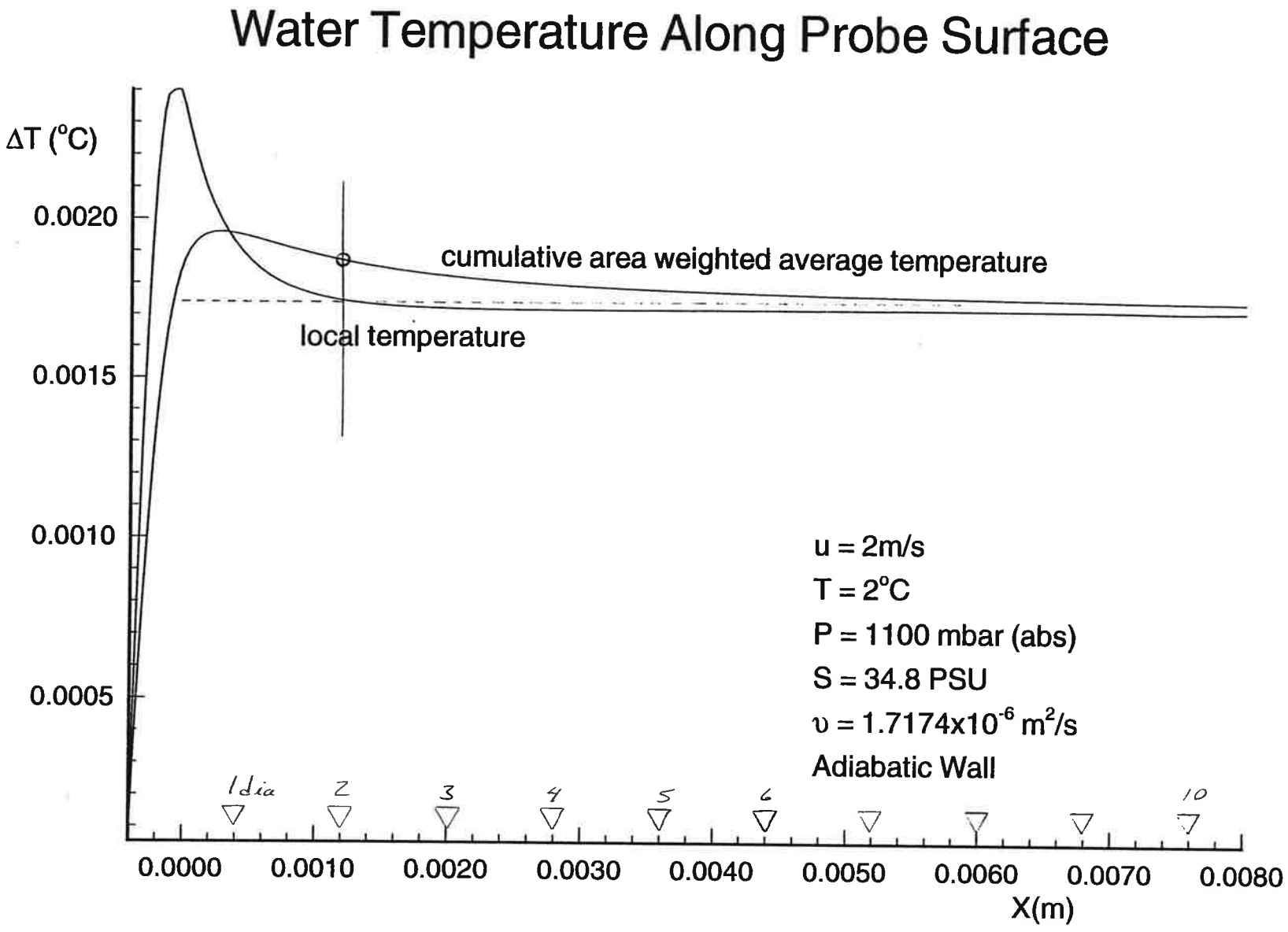
Water Temperature Along Probe Surface
ΔT (°C)
0.0020
0.0015
0.0010
0.0005
cumulative area weighted average temperature
local temperature
u = 2m/s
T = 2°C
P = 1100 mbar (abs)
S = 34.8 PSU
υ = 1.7174x10-6 m2/s
Adiabatic Wall
1dia
2
3
4
5
6
10
0.0000
0.0010
0.0020
0.0030
0.0040
0.0050
0.0060
0.0070
0.0080
X(m)

Figure 7

Cumulative Area Weighted Average Temperature Along Probe

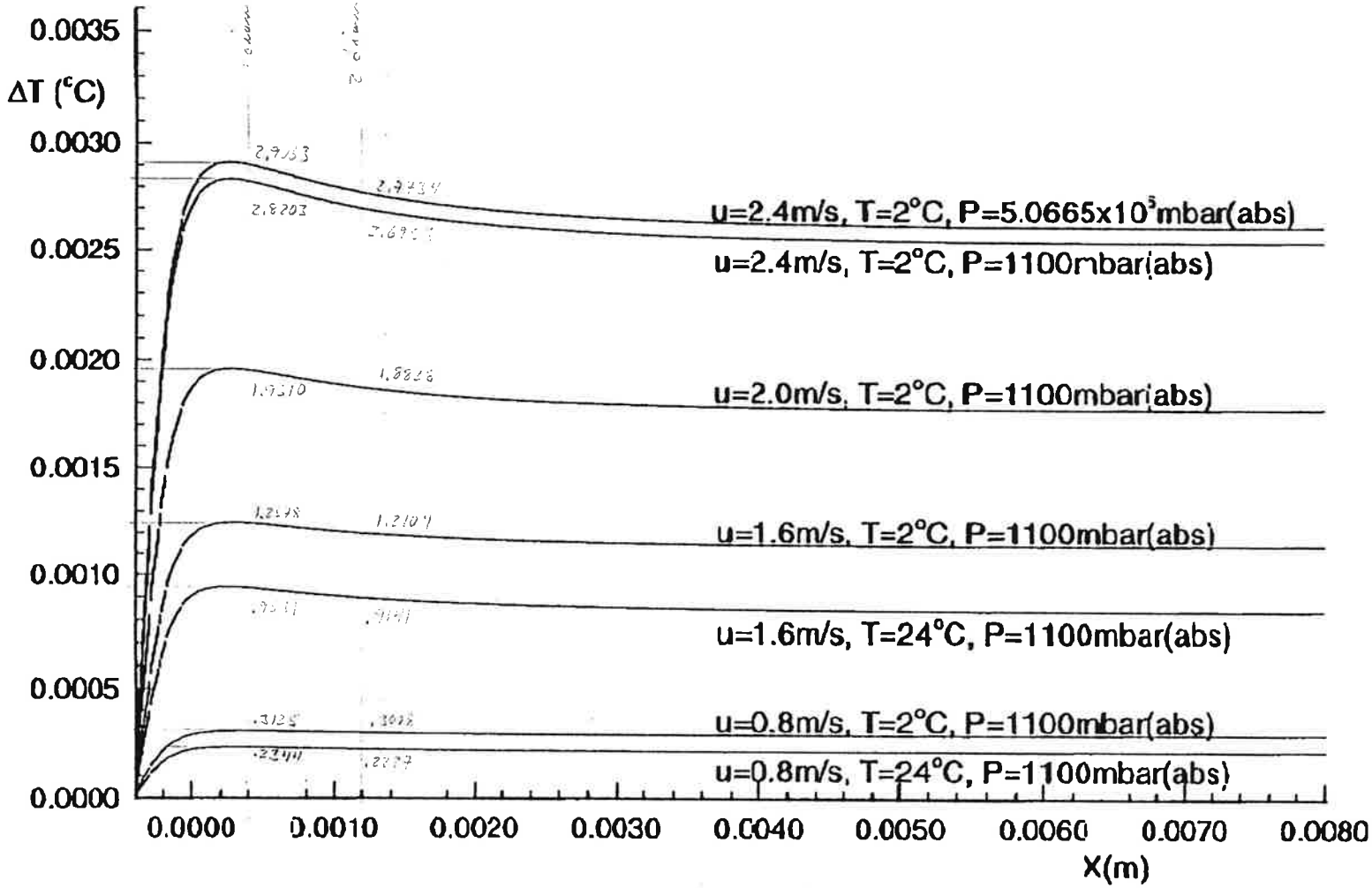

Figure 8

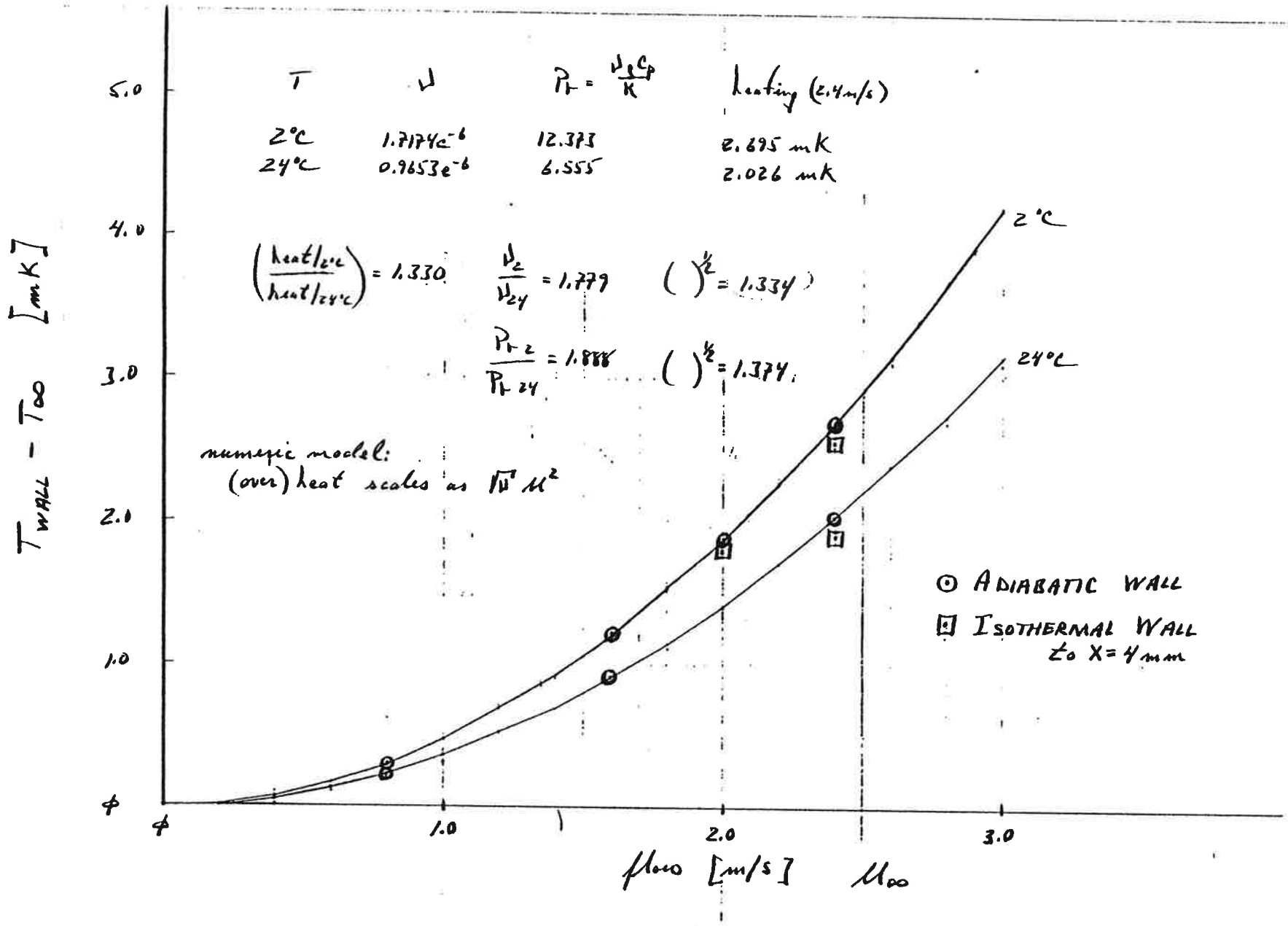
T
ν
$P_r = \frac{\nu \rho c_p}{k}$
heating (2.4 m/s)
2°C 1.7174e⁻⁶ 12.373 2.695 mK
24°C 0.9653e⁻⁶ 6.555 2.026 mK
$\left(\frac{\text{heat}/_{2°C}}{\text{heat}/_{24°C}}\right) = 1.330$
$\frac{\nu_2}{\nu_{24}} = 1.779$ $(\ )^{1/2} = 1.334$
$\frac{P_{r\,2}}{P_{r\,24}} = 1.888$ $(\ )^{1/2} = 1.374$
numerical model:
(over) heat scales as $\sqrt{\nu}\, u^2$
2°C
24°C
⊙ ADIABATIC WALL
⊡ ISOTHERMAL WALL
to X = 4 mm
$T_{WALL} - T_\infty$ [mK]
5.0
4.0
3.0
2.0
1.0
0
0
1.0
2.0
3.0
flow [m/s] u_∞

Figure 9

(A) Blunt-tip geometry. $r = \frac{R}{2}$

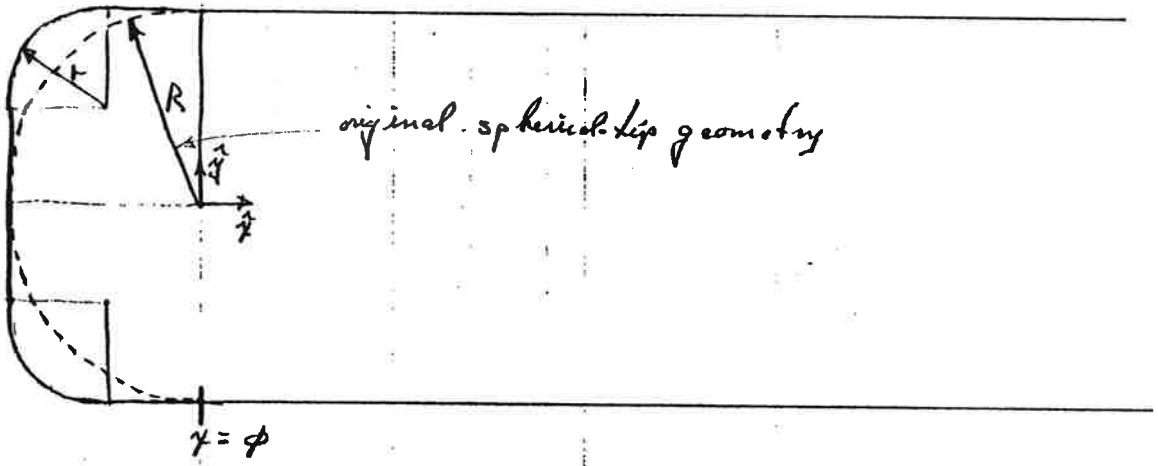

(B) elliptical-tip geometry

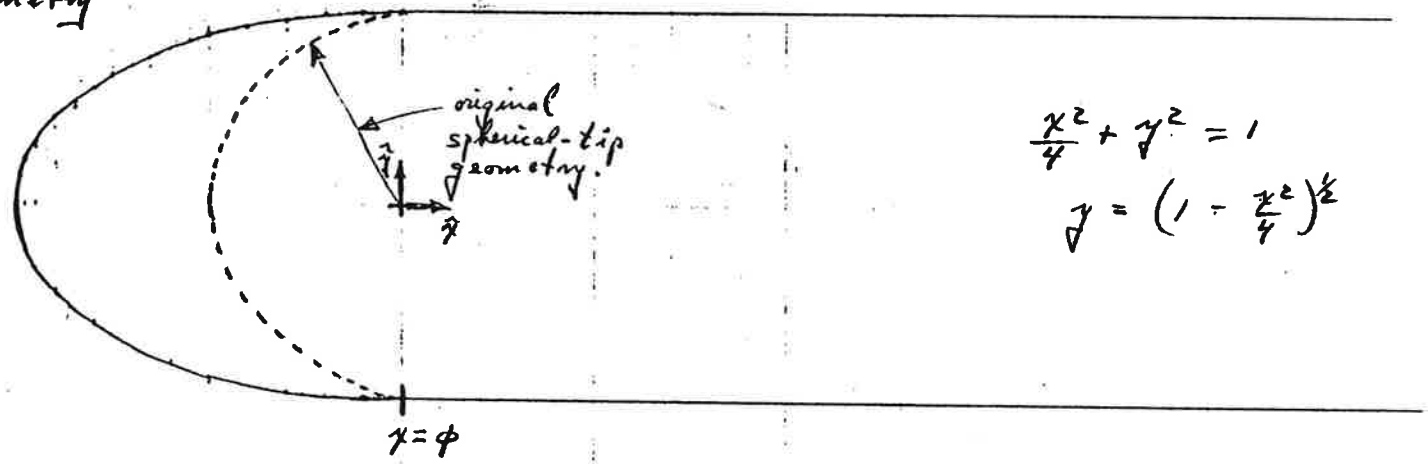

$$\frac{x^2}{4} + y^2 = 1$$

$$y = \left(1 - \frac{x^2}{4}\right)^{1/2}$$

Figure 10

Effect of Nose Bluntness on Average Wall Temperature

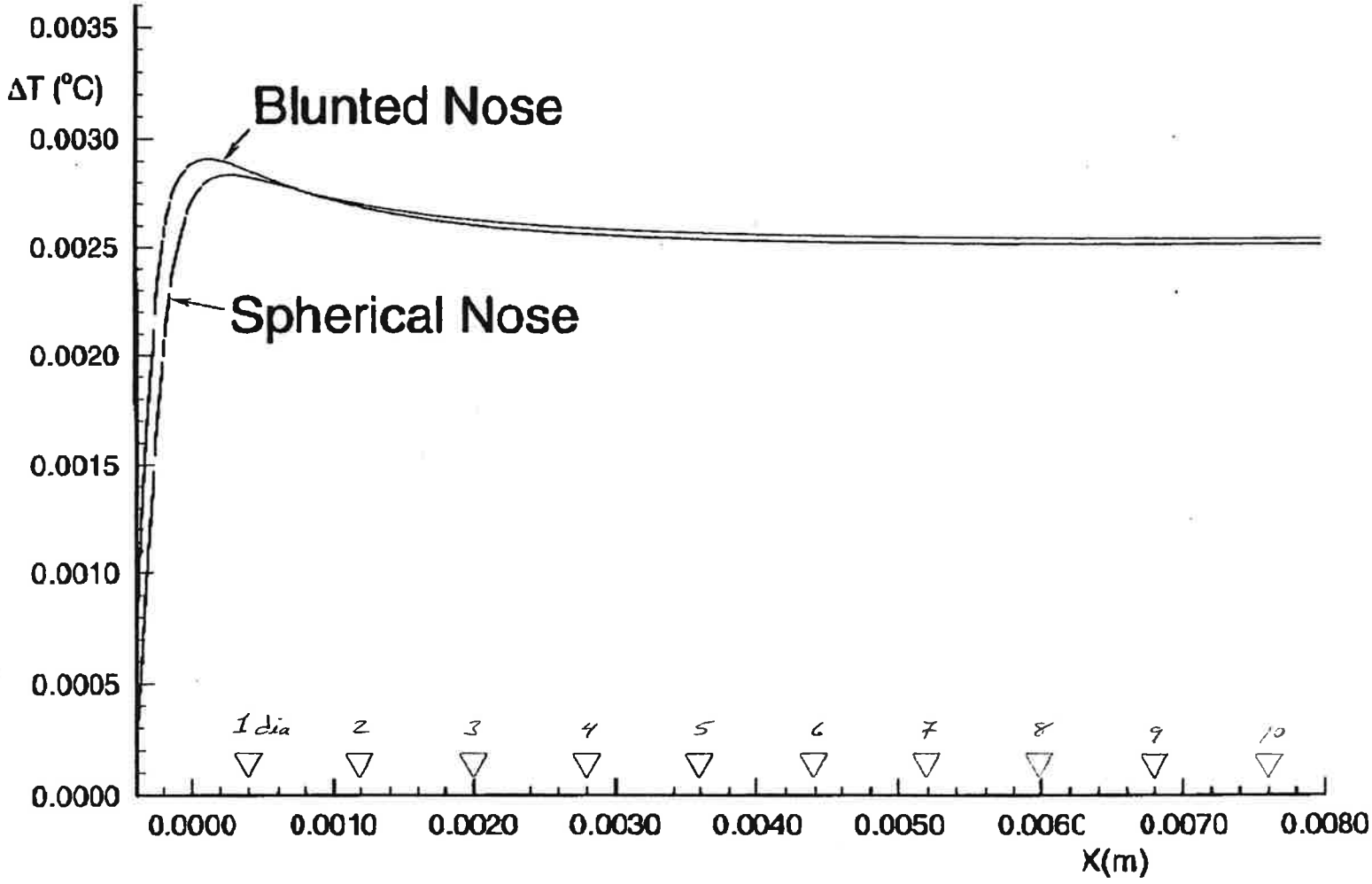

Figure 11

Heat Flux Distribution

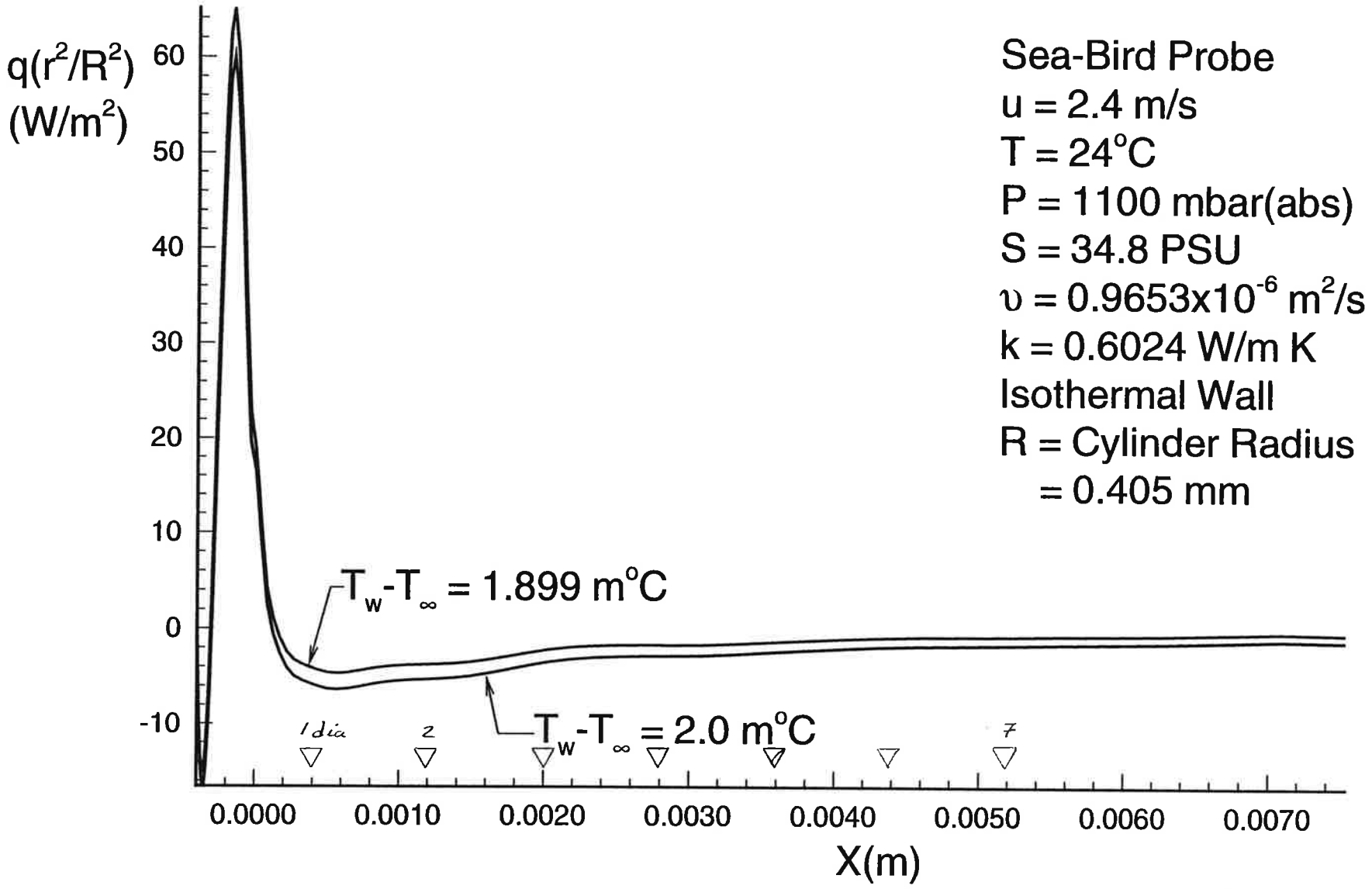

Figure 12

Integrated Wall Heat Transfer vs Wall Temperature

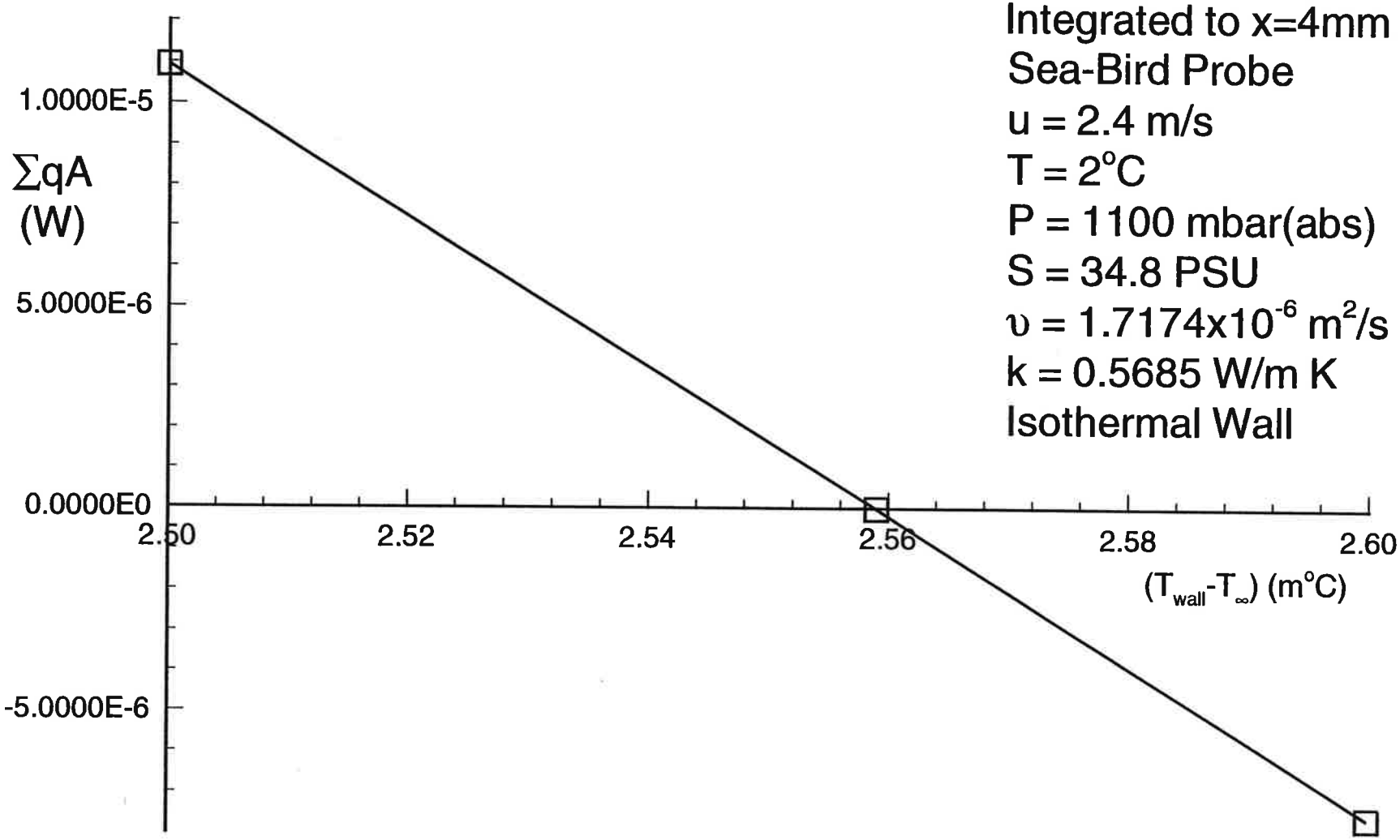

Figure 13

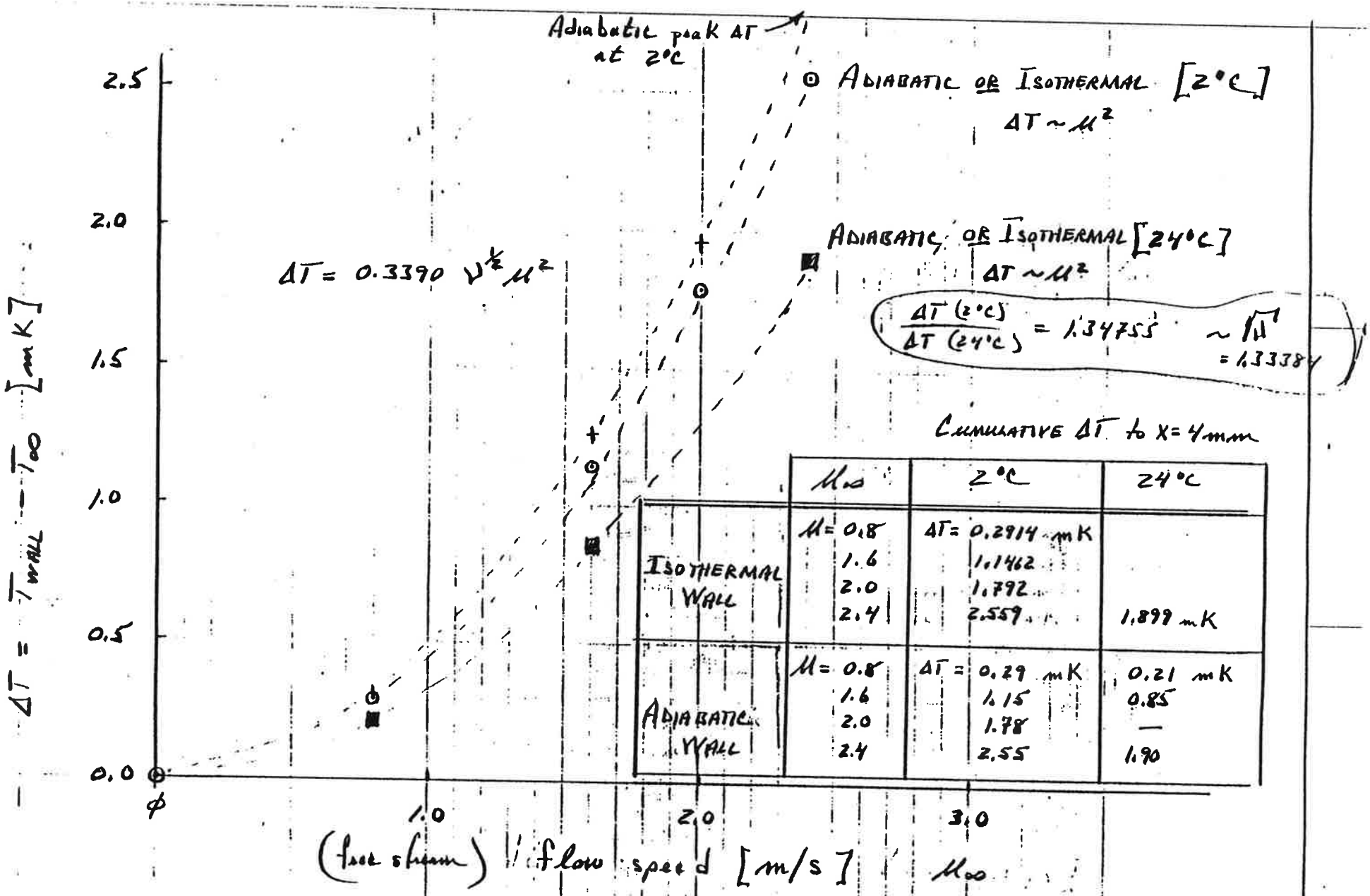
Adiabatic peak ΔT at 2°C
Adiabatic or Isothermal [2°C]
ΔT ~ M²
Adiabatic or Isothermal [24°C]
ΔT ~ M²
ΔT = 0.3390 M² M²
ΔT (2°C) / ΔT (24°C) = 1.34755 ~ 4/3 = 1.3333
Cumulative ΔT to x = 4 mm
Isothermal Wall
Adiabatic Wall
M∞ | 2°C | 24°C
M = 0.8 | ΔT = 0.2914 mK
1.6 | 1.1462
2.0 | 1.792
2.4 | 2.559 | 1.899 mK
M = 0.8 | ΔT = 0.29 mK | 0.21 mK
1.6 | 1.15 | 0.85
2.0 | 1.78 | —
2.4 | 2.55 | 1.90
2.5
2.0
1.5
1.0
0.5
0.0
1.0
2.0
3.0
M∞
− ΔT = T_wall − T∞ [mK]
(free stream) M: flow speed [m/s]

Figure 14

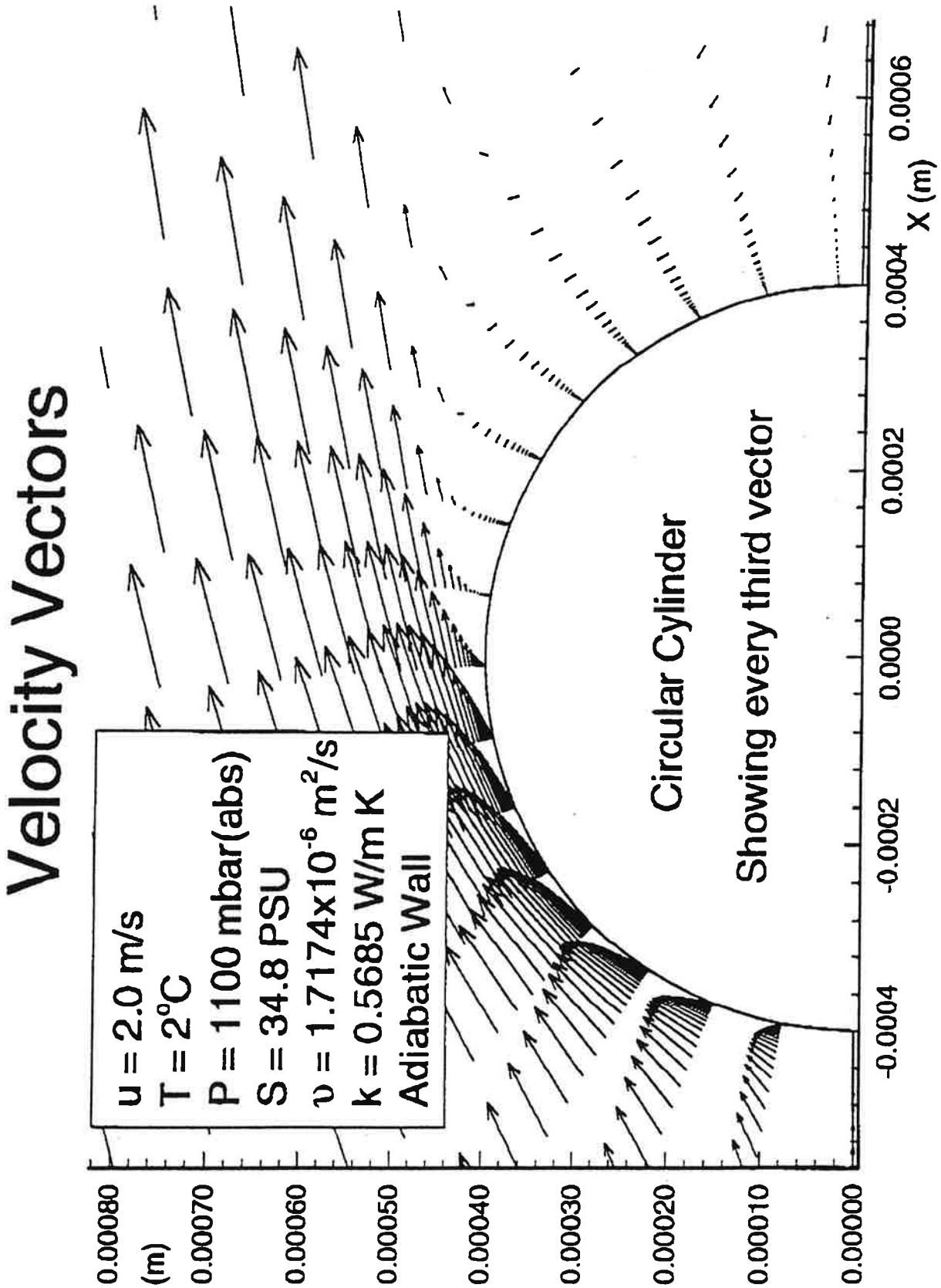
Velocity Vectors
u = 2.0 m/s
T = 2°C
P = 1100 mbar(abs)
S = 34.8 PSU
υ = 1.7174x10⁻⁶ m²/s
k = 0.5685 W/m K
Adiabatic Wall
Circular Cylinder
Showing every third vector
Y (m)
X (m)
0.00080
0.00070
0.00060
0.00050
0.00040
0.00030
0.00020
0.00010
0.00000
-0.0004
-0.0002
0.0000
0.0002
0.0004
0.0006

Figure 15

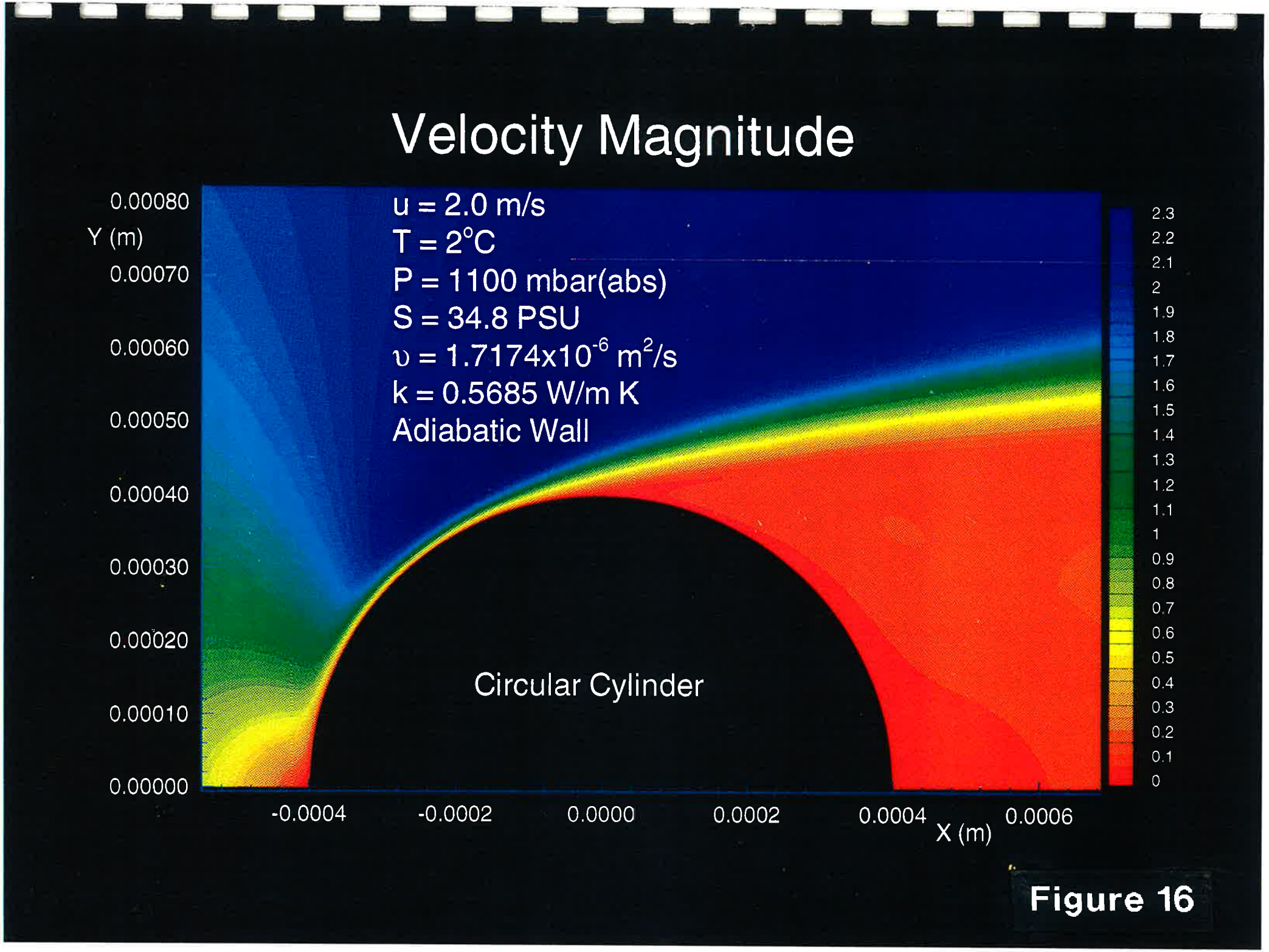
Velocity Magnitude
u = 2.0 m/s
T = 2°C
P = 1100 mbar(abs)
S = 34.8 PSU
υ = 1.7174x10^-6 m^2/s
k = 0.5685 W/m K
Adiabatic Wall
Circular Cylinder
Y (m)
0.00080
0.00070
0.00060
0.00050
0.00040
0.00030
0.00020
0.00010
0.00000
-0.0004
-0.0002
0.0000
0.0002
0.0004
0.0006
X (m)
2.3
2.2
2.1
2
1.9
1.8
1.7
1.6
1.5
1.4
1.3
1.2
1.1
1
0.9
0.8
0.7
0.6
0.5
0.4
0.3
0.2
0.1
0

Figure 16

Color Flooded Temperature Contours

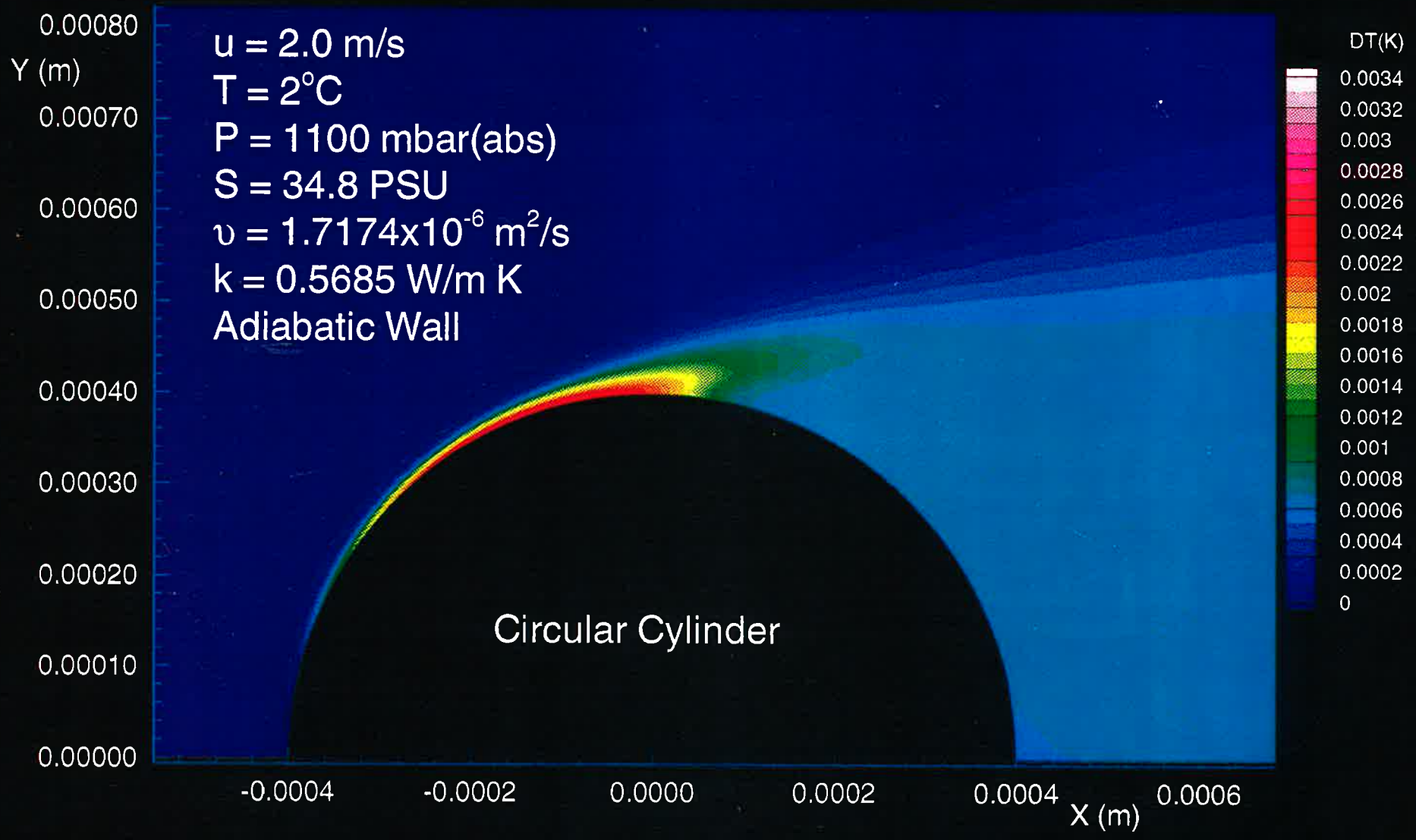

Figure 17

Water Temperature Along Probe Surface

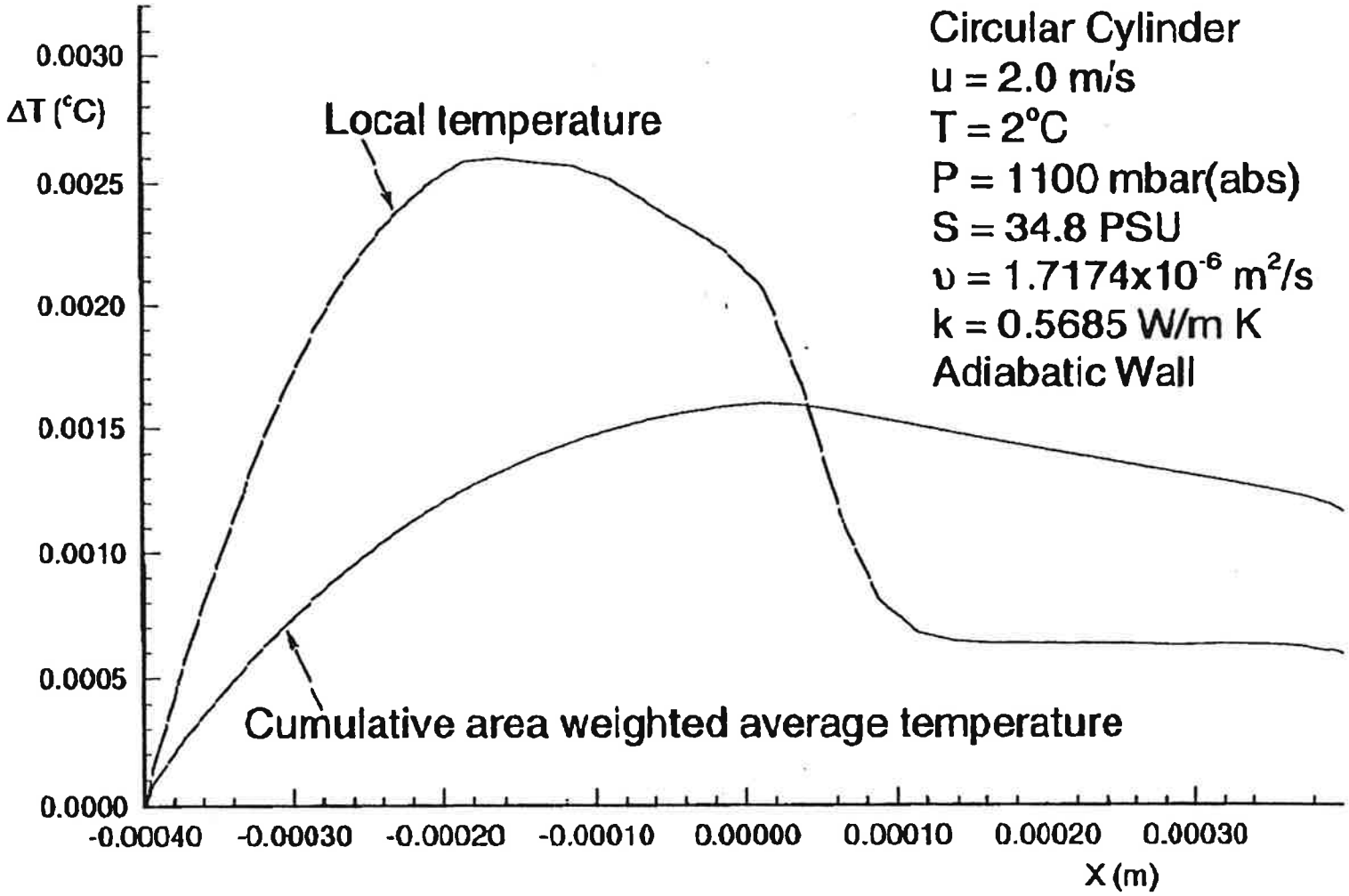

Figure 18

Heat Flux Distribution

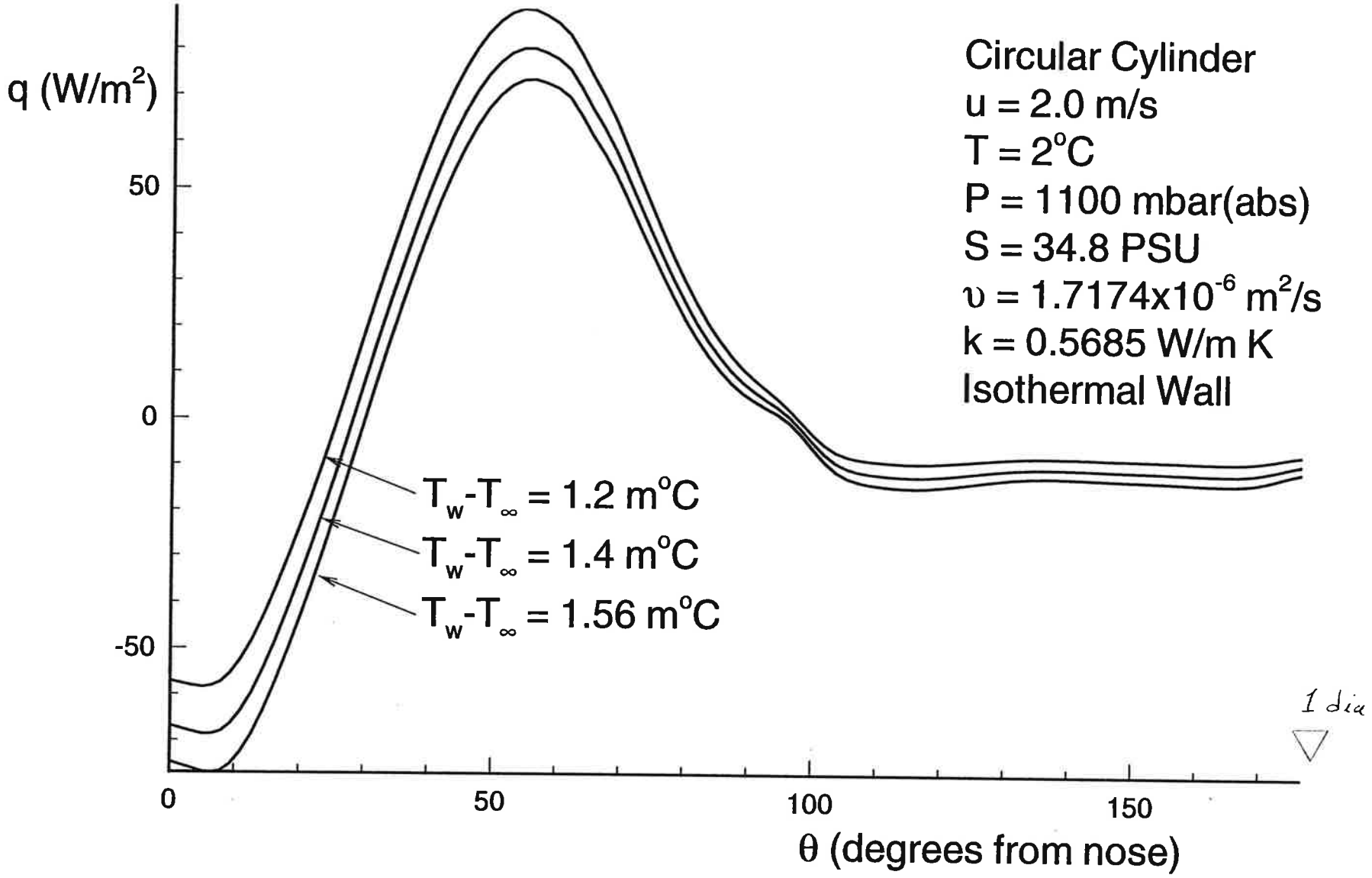

Figure 19

Variation of Integrated Wall Heat Transfer With Wall Temperature

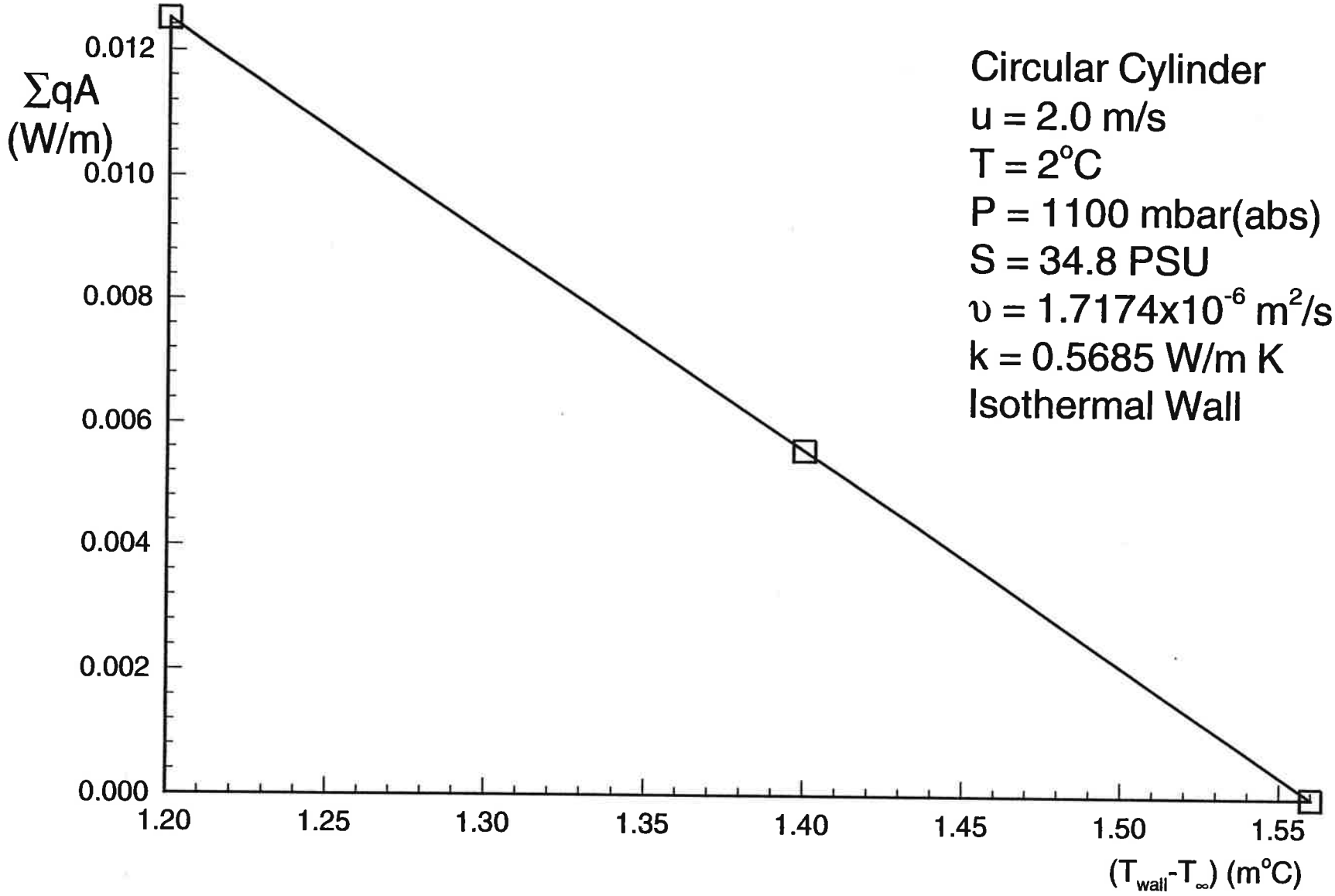

Figure 20

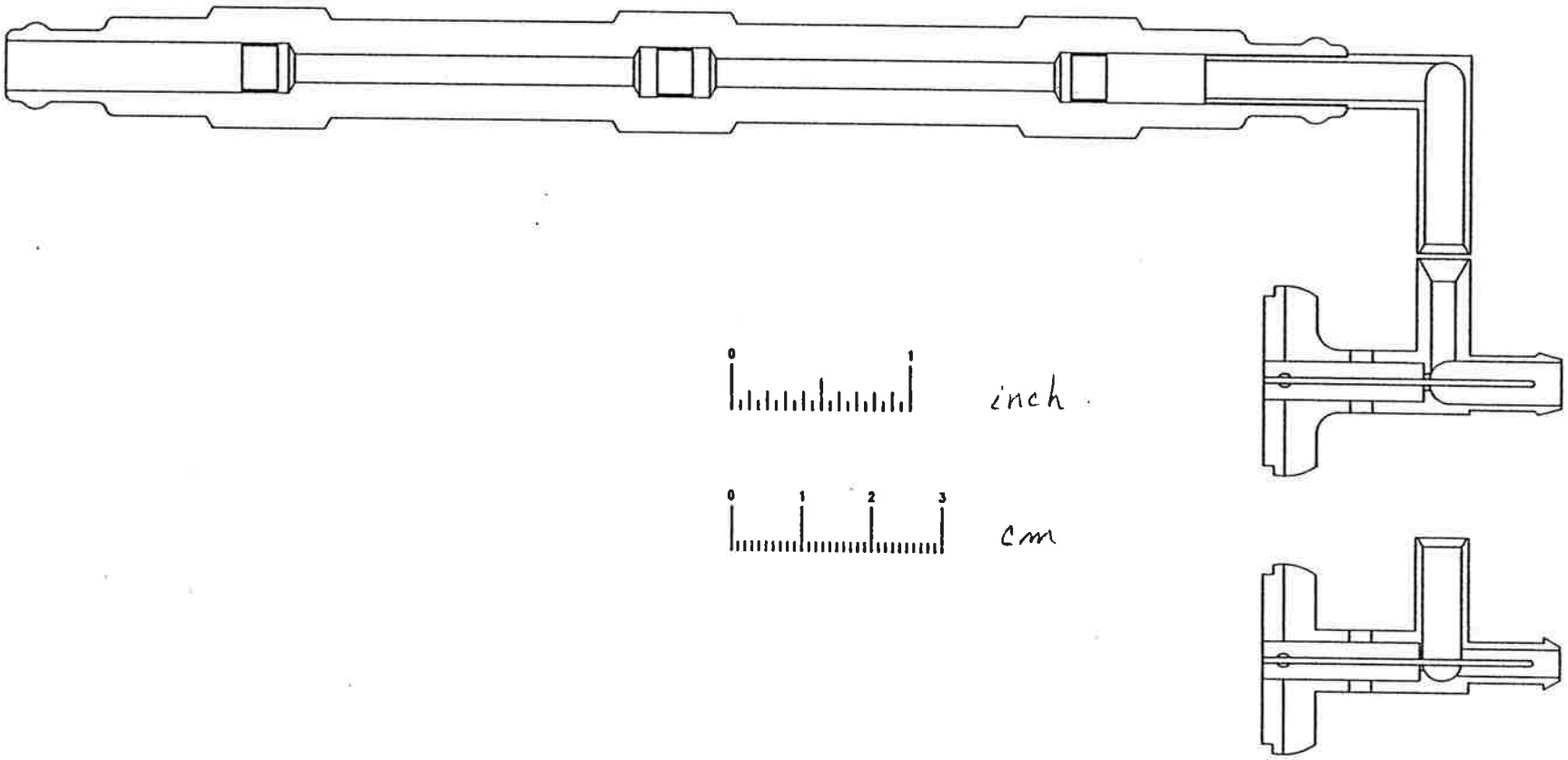

Figure 21

1509BW.CNV: viscous heating in standard TC duct

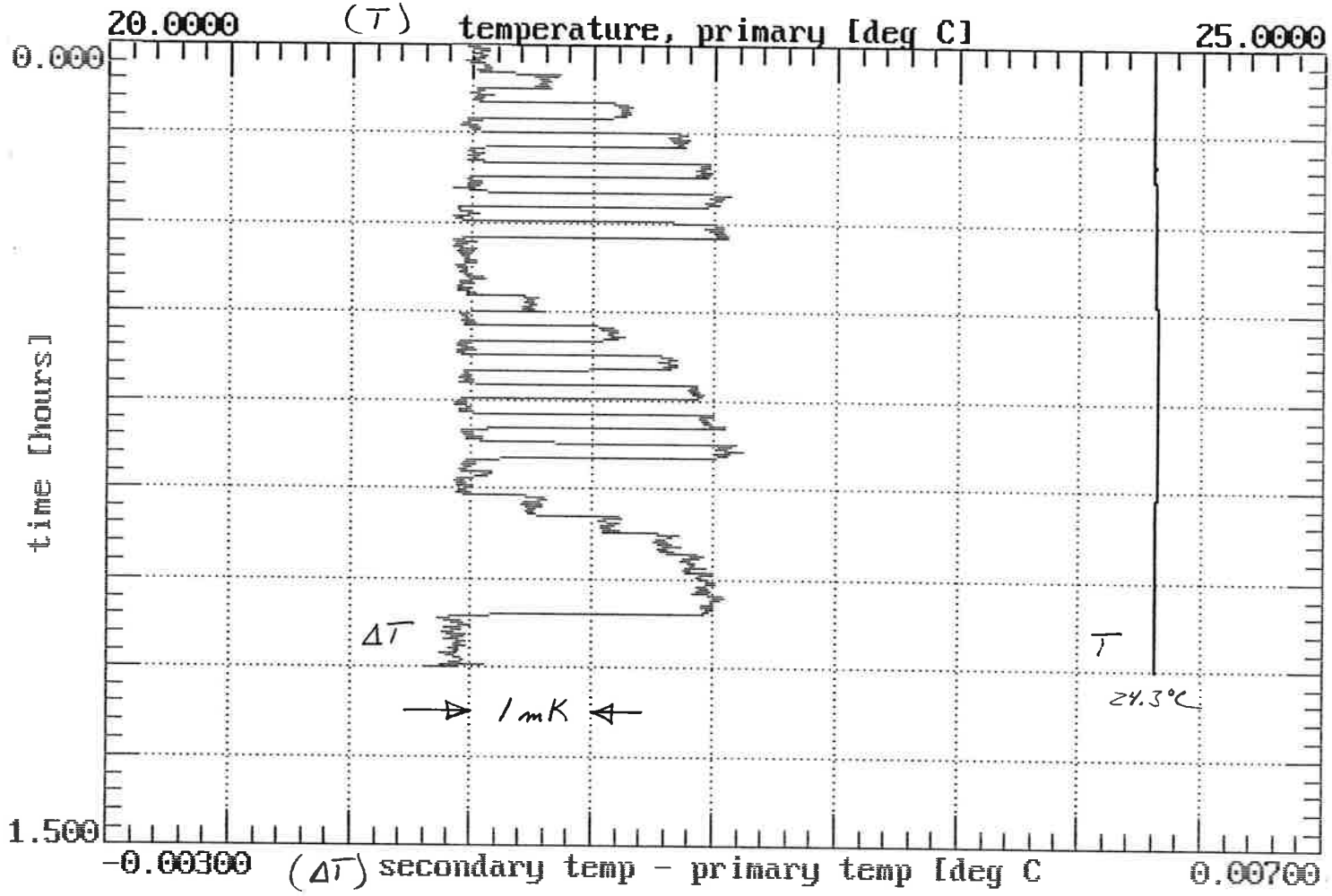

Figure 22

STANDARD TC DUCT

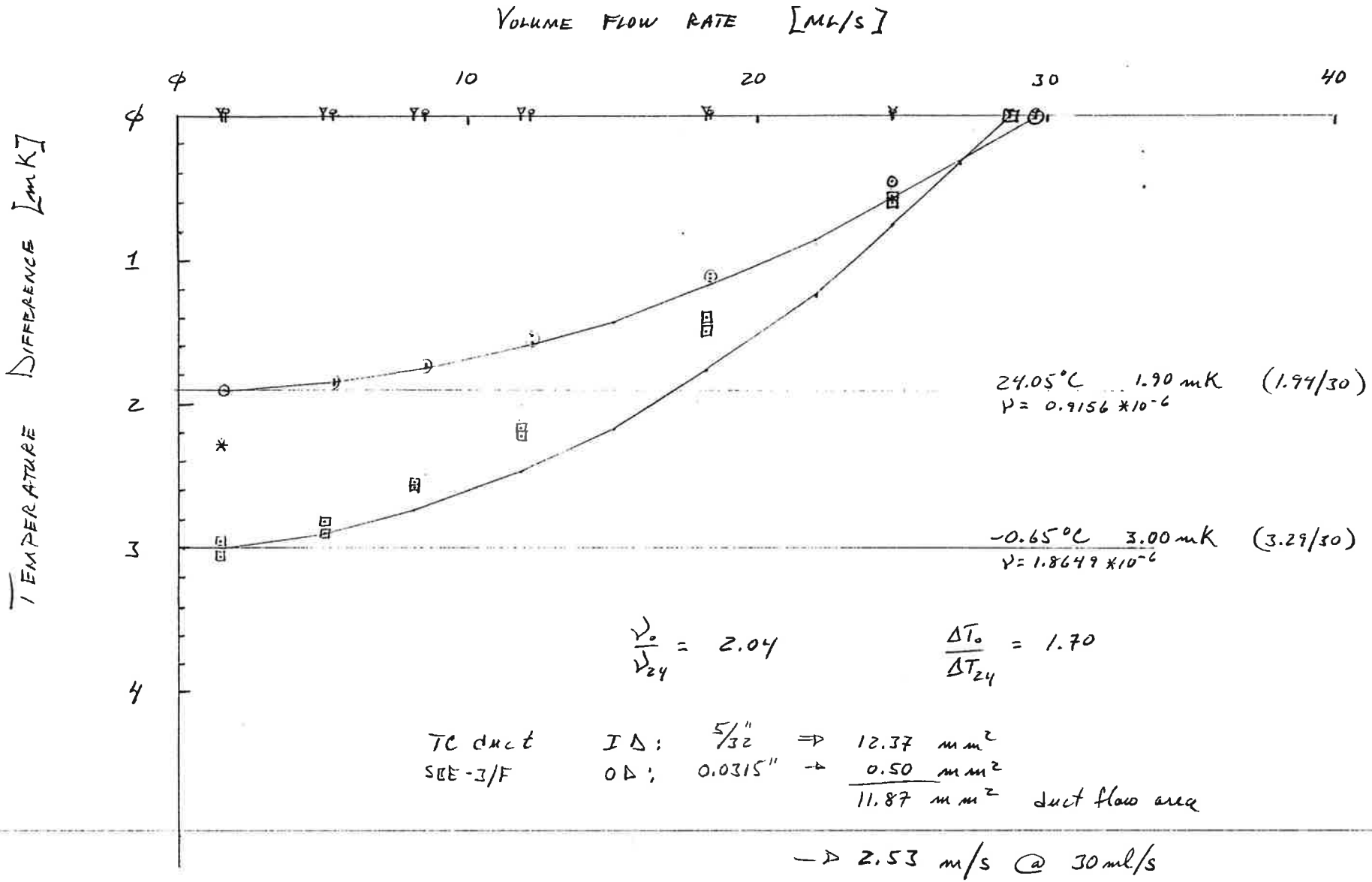

Figure 23

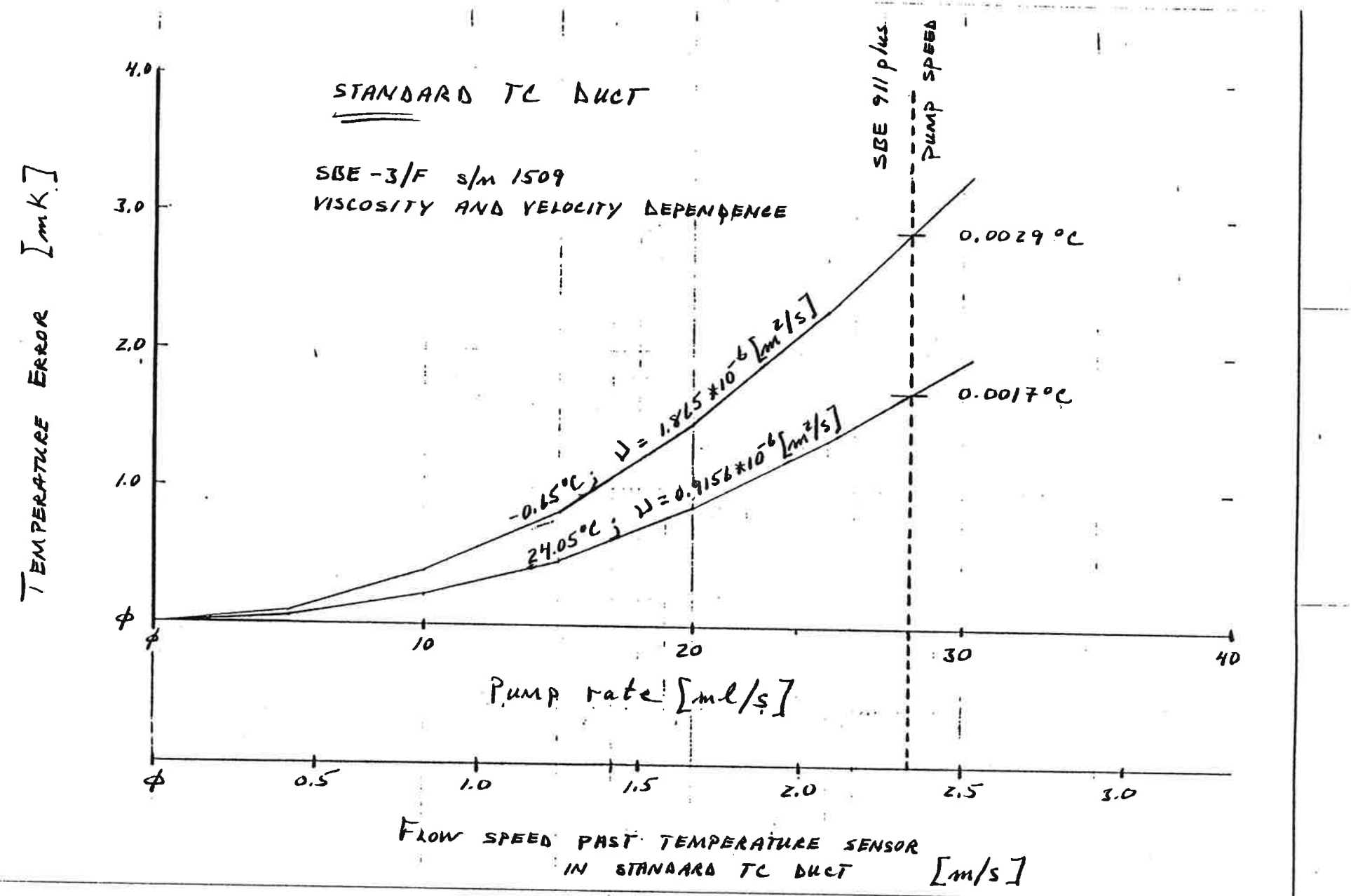
STANDARD TC DUCT
SBE-3/F s/n 1509
VISCOSITY AND VELOCITY DEPENDENCE
SBE 911 plus
PUMP SPEED
0.0029 °C
0.0017 °C
-0.65°C; ν = 1.865 *10⁻⁶ [m²/s]
24.05°C; ν = 0.9156*10⁻⁶ [m²/s]
TEMPERATURE ERROR [mK]
4.0
3.0
2.0
1.0
0
0
10
20
30
40
Pump rate [ml/s]
0
0.5
1.0
1.5
2.0
2.5
3.0
FLOW SPEED PAST TEMPERATURE SENSOR IN STANDARD TC DUCT [m/s]

Figure 24

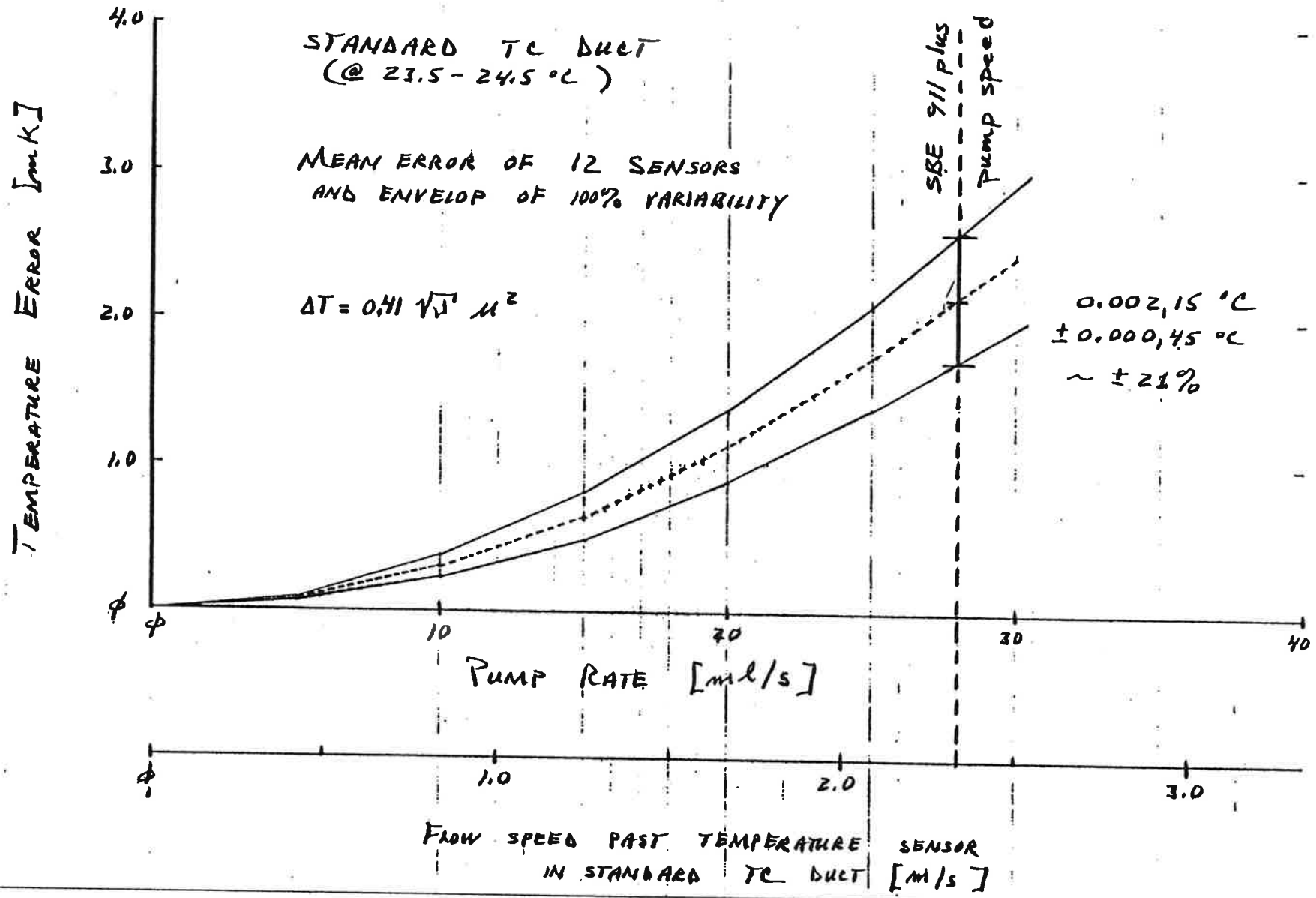
STANDARD TC DUCT
(@ 23.5 - 24.5 °C)
MEAN ERROR OF 12 SENSORS
AND ENVELOP OF 100% VARIABILITY
ΔT = 0,41 √J m²
SBE 911 plus
Pump speed
0.002,15 °C
± 0.000,45 °C
~ ± 21%
TEMPERATURE ERROR [mK]
4.0
3.0
2.0
1.0
0
0
10
20
30
40
PUMP RATE [ml/s]
0
1.0
2.0
3.0
FLOW SPEED PAST TEMPERATURE SENSOR
IN STANDARD TC DUCT [m/s]

Figure 25